Polymer 51 (2010) 748–754

Contents lists available at ScienceDirect

Polymer

journal homepage: www.elsevier.com/locate/polymer

The effect of matrix morphology on nanocomposite properties

Xiaolan Hu [a,b], R. Bradley Johnson [b], Michelle R. Schlea [b], Jasmeet Kaur [b], Meisha L. Shofner [b,*]

[a] Department of Materials Science and Engineering, College of Materials, Xiamen University, Xiamen, Fujian 361005, China
[b] School of Polymer, Textile & Fiber Engineering, Georgia Institute of Technology, 801 Ferst Drive, Atlanta, GA 30332, USA

ARTICLE INFO

Article history:
Received 11 August 2009
Received in revised form
3 December 2009
Accepted 5 December 2009
Available online 16 December 2009

Keywords:
Polymer nanocomposite
Matrix morphology
Dynamic mechanical properties

ABSTRACT

In order to understand the effect of bulk matrix morphology on polymer nanocomposite properties, nanocomposites containing chemically similar but morphologically different polyamide matrices and carbon nanofibers were processed and characterized. Two polyamide matrices were used, one amorphous and one semi-crystalline. Experimental results indicated that the reinforcing efficacy of the amorphous matrix was higher than the semi-crystalline matrix at temperatures below the glass transition. At a carbon nanofiber loading of 0.5 wt.%, the experimentally measured modulus with the amorphous matrix exceeded the Halpin-Tsai prediction for an isotropic material. Overall, these results provided distinct evidence that the underlying bulk matrix morphology plays an important role in polymer nanocomposite mechanical design.

1. Introduction

Polymer nanocomposites have been materials of interest for over 100 years, beginning with research concerning filled elastomers and the relevant reinforcement mechanisms in these systems. In the past 20 years, renewed interest in nanocomposites has been prompted by research from the Toyota Central Research and Development Labs concerning molecular composites containing nanoclay with drastically improved mechanical and thermal properties at unconventional filler levels in the late 1980s and early 1990s [1–4] and Iijima's widely cited article in Nature concerning carbon nanotubes [5]. These developments have led to the extensive research in the area of polymer nanocomposites that has shown interesting and surprising changes in physical properties at low nanofiller loadings such as changes in the glass transition temperature (T_g) that may be correlated to interfacial volume [6,7], filler network formation at low loadings [8], and decreased viscosity when entropic forces are allowed to dominate [9]. Such results motivate further studies to elucidate the mechanism responsible for these property changes, and much of this research has focused on the structure of the nanofiller/polymer interface as a possible explanation.

Since the surface area to volume ratio of nanoparticles can be three to four orders of magnitude larger than particles with dimensions on the micrometer scale, the amount of surface area present in the polymer is significantly larger than that present in a composite containing microscale particles at the same loading. The additional surface area provides increased opportunity for polymer–particle interactions and changes to polymer conformation in the interfacial zone. Attempts to understand the structure of the polymer surrounding the nanoparticle have centered primarily on changing the chemistry of the system through nanoparticle surface functionalization and making comparisons between nanocomposites with different nanoparticle surface chemistry [8,10–13]. These studies provide useful insight into the strength of the interfacial interaction based on the results of materials characterization. However, the results are often difficult to deconvolute since different levels of nanoparticle dispersion may be obtained in systems where the chemical compatibility between the matrix and the nanoparticle is different.

Of the nanoparticle systems used to make nanocomposites, carbon nanofibers (CNF) offer an attractive balance of multifunctional properties and economy. CNFs consist of graphene planes oriented in a tree ring structure around a hollow core. However, CNFs are structurally different than nanotubes. The CNF diameter is built up from the hollow core by chemical vapor deposition instead of consisting of a concentric array of carbon cylinders. As a result, these fibers generally have a larger amount of defects causing their property values to be lower than carbon nanotubes, and CNF properties are also highly dependent on the orientation angle of the graphene planes [14]. CNFs have been used as reinforcing agents in a number of polymer matrices including acrylonitirile-co-butadiene-co-stryrene [15,16], polyamide [17,18], polypropylene [19–21] [17,18], polyester (PET) [22], polyetherimide [23,24], polyethylene [25,26], polymethylmethacrylate (PMMA) [27–29], polystyrene [30–32], and thermoplastic elastomers [33]. In these

* Corresponding author. Tel.: +1 404 385 7216; fax: +1 404 894 8780.
E-mail address: meisha.shofner@ptfe.gatech.edu (M.L. Shofner).

0032-3861/$ – see front matter © 2009 Elsevier Ltd. All rights reserved.
doi:10.1016/j.polymer.2009.12.006

systems, CNFs have generally provided mechanical property increases and, at sufficient CNF loadings, electrical conductivity. Additionally, like other nanofillers, CNFs have the capability of simultaneously strengthening and toughening polymer matrices. Isotropically oriented CNF/polyethylene composites with high levels of dispersion and strong interfacial interactions possessed increased tensile modulus and strain to failure with minimum increases of 60% and 220% in modulus and strain to failure, respectively at a filler loading of 8 wt.% [25].

Bulk polymer morphology should have an effect on the reinforcing mechanism of nanoparticles, but it has not been explored extensively. Although a self-contained, comprehensive study was not available in the literature concerning the effect of polymer morphology on CNF composite properties, the combination of separate studies from the Kumar research group concerning CNF fibers indicate that polymer morphology was a factor in the reinforcing efficacy of CNF composites. Nanocomposite fibers containing 5 wt.% CNF showed larger tensile property increases when an amorphous polymer matrix was used as compared to a semi-crystalline matrix below T_g [22,27]. In both systems, similar levels of CNF dispersion and alignment were attained. CNF fibers with a PMMA matrix showed greater than 50% improvement in tensile modulus. Similar research with a PET matrix showed no significant increase in tensile modulus at the same CNF loading. Additionally, both systems showed improvements in compressive modulus, but the enhancement was greater in the PMMA system. Taken together, these studies indicated that in addition to engineered compatibility between nanocomposites components through nanoparticle surface chemistry, matrix structure could have an influence on the nanocomposites properties.

In this paper, we have prepared and characterized two CNF nanocomposite systems using chemically similar polymer matrices with different inherent morphologies, amorphous and semi-crystalline. This experimental design was chosen to mitigate issues of nanoparticle dispersion and to help isolate the contribution of matrix morphology on nanocomposite reinforcement. The results of this research provided experimental evidence that an amorphous matrix achieved a higher percentage of reinforcement than a semi-crystalline matrix below T_g when the underlying matrix structure was not changed by the inclusion of CNFs. Additionally, reinforcement levels exceeding the Halpin-Tsai prediction for an isotropic material were achieved at low nanofiller loadings in the amorphous matrix. These results suggested that the polymer morphology could impact nanocomposite performance and provide another parameter for nanocomposite design.

2. Experimental section

The composites processed and characterized in this research contained CNFs and polyamide (PA) matrices. The CNFs were donated by Pyrograf Products (Cedarville, Ohio). Their product designation was PR-24-PS. According to the manufacturer, these CNFs had diameters in the range of 60–150 nm and lengths in the range of 30–100 μm. The CNFs were cleaned from the as-received condition using a procedure from Lozano *et al.* [34]. Briefly, the procedure involves a five day reflux in methylene chloride followed by washing with deionized water and an additional one day reflux step in deionized water. This treatment introduces hydroxyl, hydrocarbon, carboxyl, and quinone groups on the CNF surface. It has been shown previously to aid in CNF dispersion in polymer composites [15,16,20,21,25]. The polymer matrices were an amorphous PA 6,10 (Isocor™ CN30BT) and a semi-crystalline PA 6,10 (Isocor™ 6100) that were donated by Shakespeare Polymers (Columbia, South Carolina). PA was chosen for this research because it is a widely used class of engineering thermoplastics that is available in amorphous and semi-crystalline forms, allowing the effects of matrix morphology on nanocomposite interfacial structure to be studied explicitly. In this paper, the amorphous and semi-crystalline polyamides are designated A-PA and SC-PA, respectively. The A-PA is a copolymer with polyamide 6,10 and polyamide 6I where the aromatic polymer inhibits crystallization. The MSDS lists the polyamide 6I content at 40–60%.

The nanocomposites were prepared by melt-mixing. CNF loadings of 0.5, 1 and 3 wt.% were used in both matrices. Neat polymer samples of both matrices were prepared by the same processing protocol for comparison to the nanocomposites. Prior to mixing, the PA pellets were dried in a vacuum oven for 24 h to minimize hydrolytic degradation during processing. The A-PA pellets were dried at 60 °C, and the SC-PA pellets were dried at 80 °C. These temperatures were recommended by the processing datasheets from the manufacturer. The materials were mixed using a three piece mixer attached to Brabender Intelli–Torque drive. The mixer had roller blades and a 60 mL capacity. In all materials processed here, the overall batch weight was kept constant at 50 g. The A-PA materials were mixed at a set temperature of 200 °C for 10 min, and the SC-PA materials were mixed at a temperature of 220 °C for 10 min. All materials were processed under a flowing nitrogen atmosphere. The mixing speed used was 60 rpm for 9 min and 90 rpm for the last minute. After mixing, the materials were pressed into sheets using compression molding. The mold was heated to 200 °C and 230 °C for the A-PA and the SC-PA, respectively. All materials were pressed at 5 ton for 8 min. The materials were removed from the press immediately and placed on the benchtop to cool in the mold. A weight was placed on top of the mold until the material's temperature was below the polymer's T_g.

The dispersion and distribution achieved in the nanocomposites was observed with scanning electron microscopy (SEM). SEM imaging was performed with a LEO 1530 SEM using fracture surfaces. All samples were sputter coated with gold prior to SEM imaging. Thermal analysis was performed on the nanocomposites and the neat polymers using differential scanning calorimetry (DSC). DSC experiments were conducted using a TA Instruments DSC Q100. Samples were heated at 10 °C/min from zero to 250 °C and cooled at the same rate in a flowing nitrogen environment. Information concerning polymer crystallinity and T_g was obtained using the DSC data for both matrix systems. The second heating and cooling DSC traces were used for analysis on the SC-PA samples. The first heating cycle was used to determine the crystallinity of the SC-PA materials tested mechanically.

Mechanical properties were measured using dynamic testing. Dynamic mechanical analysis (DMA) was performed in shear using a Mettler Toledo DMA/SDTA 861^e. The experiments were performed using a double shear sandwich fixture with specimens cut from the molded sheets. The samples were heated from 25 to 140 °C at a rate of 2 °C min at a frequency of 1 Hz. A force amplitude of 3 N was used below T_g, and a displacement amplitude of 2 μm was used above T_g for the A-PA composites. For the SC-PA composite materials, a force amplitude of 5 N was used below T_g, and a displacement amplitude of 1 μm was used above T_g. These parameters were in the linear viscoelastic range for the samples, determined from strain sweeps at 25 °C and 140 °C. At least two samples from each material were tested for reproducibility of the test results.

3. Results

As shown in Fig. 1, the CNF composites possessed similar distribution and dispersion in the two matrix systems at the CNF loadings studied. The CNFs were dispersed and distributed to the

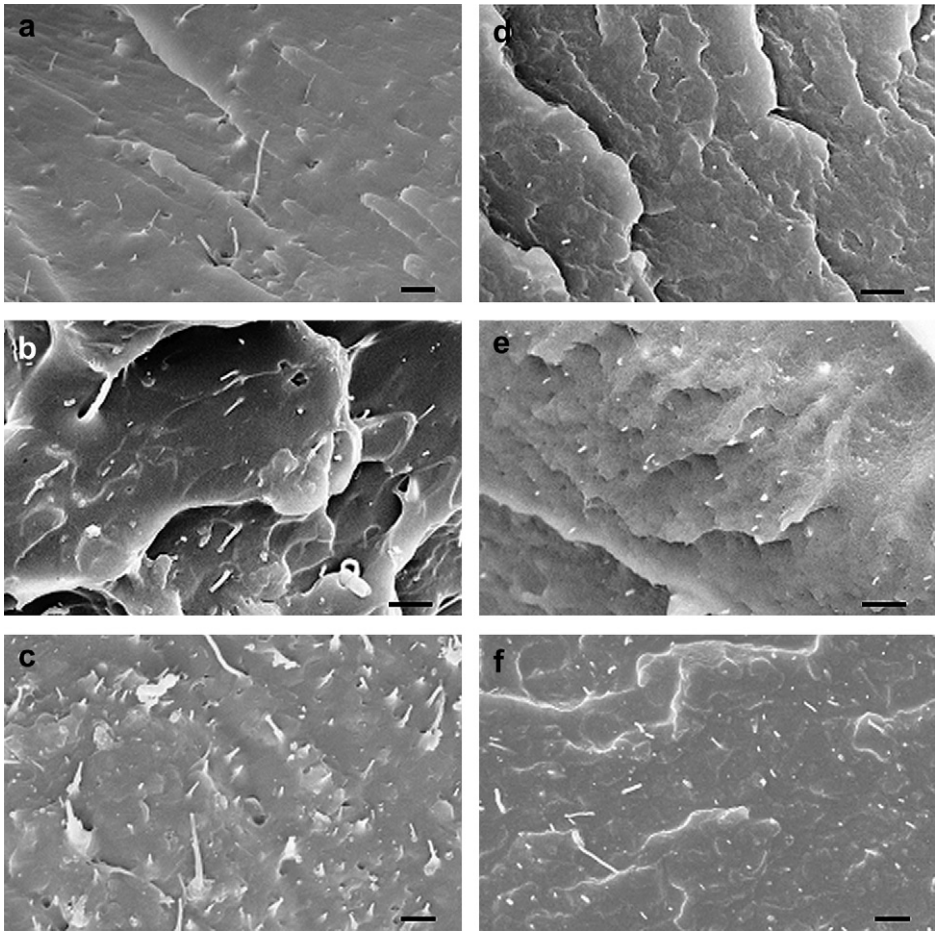

Fig. 1. SEM images of CNF composite materials. A-PA matrix materials are shown in the left column with (a) 0.5 wt.% CNF, (b) 1 wt.% CNF, and (c) 3 wt.% CNF. SC-PA matrix materials are shown in the right column with (d) 0.5 wt.% CNF, (e) 1 wt.% CNF, and (f) 3 wt.% CNF. The scale bar in all images represents 2 μm.

single fiber level in the SEM images. Only one sample, 0.5 wt.% CNF/SC-PA, showed some evidence of limited CNF aggregation, but the majority of the fracture surfaces imaged for this composition showed fully dispersed and distributed CNFs. In all samples, exposed CNFs were present at the fracture surface. The SC-PA composites had shorter exposed lengths of CNFs present at the fracture surface with respect to the A-PA composites. Additionally, the SC-PA composites showed decreased fiber pull-out. Since the chemical interaction should be similar, the changes visible at the fracture surface were attributed to increased matrix rigidity and mechanical interlocking in the SC-PA composites. Overall, the dispersion and distribution achieved was largely homogeneous and similar between the two matrix systems at each concentration allowing for an increased understanding of the effect of matrix morphology on the nanocomposites' properties.

DSC experiments showed that the addition of CNFs had little impact on the matrix morphology of the A-PA and SC-PA. Fig. 2 contains a portion of the first heating cycle curve for the A-PA polymer and composites. In the temperature range shown, 140–200 °C, an endothermic dip in the heat flow curve was observed for all of the materials, and it was more pronounced for the composite materials. This event was attributed to matrix crystallinity. Though the A-PA copolymer is typically amorphous, some crystallization is possible. The peak of the melting event occurred at approximately 170 °C, whereas the neat SC-PA had a peak melting temperature of 223 °C. The large difference in these melting temperatures suggested that the crystals formed in the A-PA

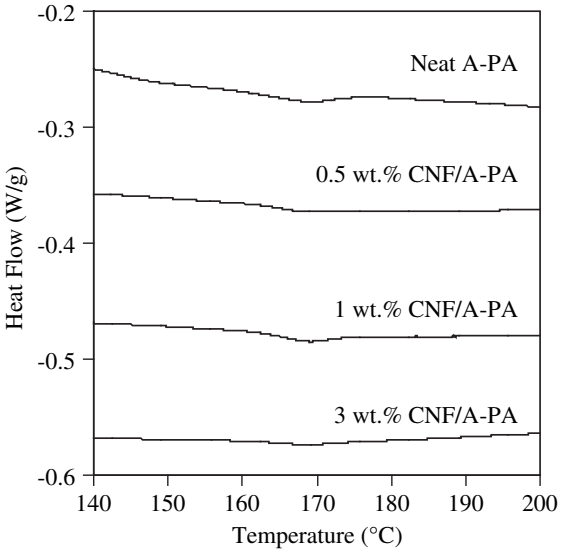

Fig. 2. DSC scans of first heating cycle of CNF/A-PA composites. During the first heating cycle, all materials showed a melting event attributed to a small amount of crystallinity generated in the matrix during cooling after processing. The amount of crystallinity did not vary widely between samples and accounted for less than 1% crystallinity. Note: Individual curves are offset for clarity.

Table 1
Features from DSC data for SC-PA and CNF/SC-PA composites during the second heating and cooling cycle.

Property	Neat SC-PA	CNF/SC-PA Composites		
		0.5 wt.%	1 wt.%	3 wt.%
Onset T_m (°C)	217 ± 0	216 ± 0	216 ± 0	215 ± 0
Peak T_m (°C)	223 ± 0	223 ± 0	223 ± 1	222 ± 0
Onset T_c (°C)	201 ± 0	203 ± 0	204 ± 0	206 ± 0
Peak T_c (°C)	198 ± 0	199 ± 0	200 ± 0	201 ± 0
% Crystallinity (second heat)	39 ± 2	39 ± 1	39 ± 0	40 ± 0
T_g (°C)	55 ± 1	52 ± 1	52 ± 0	54 ± 0

were small. The integrated area of the peak corresponded to less than 0.5% crystallinity using the heat of fusion value for polyamide 6,10 (215 J/g) [35] and assuming that 50% of the copolymer was polyamide 6I. This melting event was not observed on the second heating cycle where the material was cooled sufficiently rapidly to prevent any crystallization. Additionally, T_g showed no appreciable change with the addition of CNFs. The neat A-PA matrix has a T_g of 68 °C, and the T_g of all of the CNF composite materials were 66–67 °C.

Similarly, the morphology of the SC-PA matrix was largely unaffected by the addition of CNFs during the second heating cycle, but some changes in the kinetics of the crystallization process were suggested from the DSC cooling cycle. Table 1 contains the data for features in the DSC curves. No dramatic changes in the polymer morphology were seen when considering T_g, the melting temperature, and % crystallinity. T_g for all of the SC-PA composites was slightly lower than the neat material but within 3 °C. Larger deviations from the neat polymer's T_g were seen in the composites containing 0.5 wt.% and 1 wt.% CNF loading. The onset and peak melting temperatures were within 2 °C of the neat value, and the melting enthalpy indicated that the matrix crystallinity in the CNF composites was within 2% of the value for the neat SC-PA during the second heating cycle. However, the crystallization of the nanocomposites containing CNFs began at a higher temperature than the neat SC-PA. Both the onset and peak crystallization temperatures systematically increased with CNF content as shown in Fig. 3. At 3 wt.% CNFs, the onset crystallization temperature was 5 °C higher than the neat SC-PA. The increased crystallization temperature suggests that the CNFs have a nucleating effect on the matrix. The nucleating effect could have resulted from increased polymer viscosity allowing stable nuclei to form at higher temperatures or from the increasing amount of surface area available as the CNF concentration increased. Since morphological changes were not apparent in the melting event, the increased crystallization temperatures observed in the composites were likely a result of increased polymer viscosity.

The DMA results indicated that there was a clear difference between the reinforcement provided by the CNFs in the two matrices studied here. Figs. 4 and 5 show the G' and G'' data for the A-PA and SC-PA matrices, respectively. In the A-PA matrix, all of the composites showed higher storage modulus before T_g with the largest reinforcement in this temperature range for all materials at 30 °C. The increase in storage modulus at this temperature was similar between the composites with the 0.5 wt.% and 3 wt.% CNF composites showing an increase of 37% and 36% with respect to the neat polymer, respectively. The increase in G' for the 1 wt.% CNF composite was not outside the bounds of experimental error. Above T_g, negligible or negative reinforcement was observed until 125 °C where crystallization of all materials began to occur. The crystallization event was indicated by the increase in G' and G''. Since the neat polymer also showed crystallization, the event was not

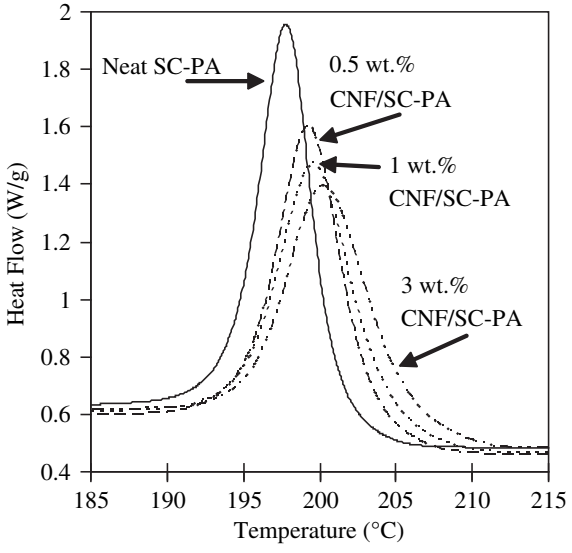

Fig. 3. Crystallization of SC-PA materials during the DSC second cooling cycle (Heating and cooling rates were 10 °C/min). The addition of CNFs to the SC-PA matrix systematically increased the onset and peak crystallization temperature. The increased crystallization temperature suggests that the CNFs aided nucleation in this system.

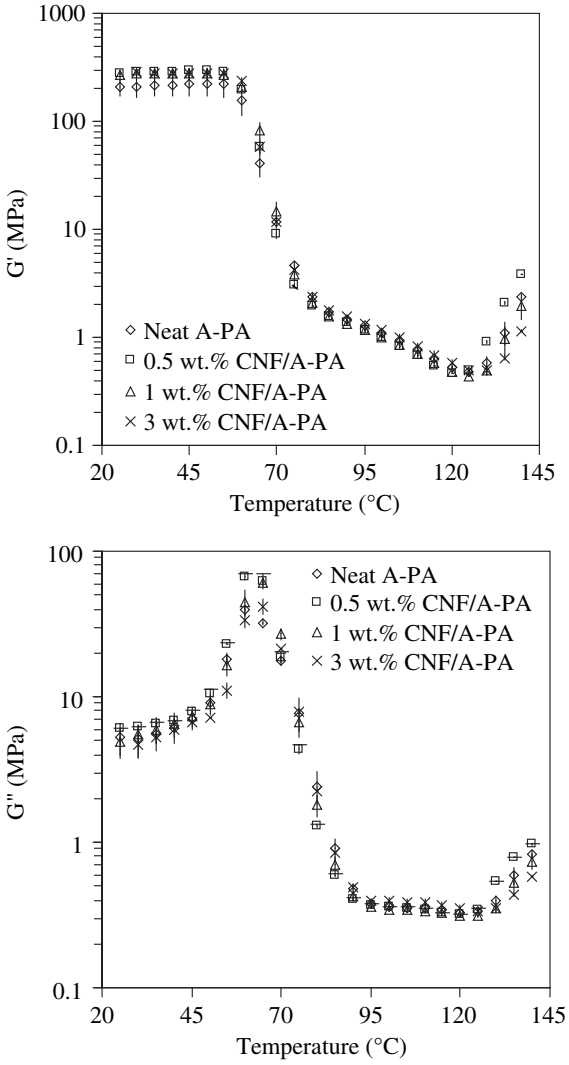

Fig. 4. DMA results for A-PA materials. Reinforcement of the matrix was seen at temperatures below T_g for G′ and in the vicinity of T_g for G″. At approximately 125 °C, the value of G′ and G″ increased due to matrix crystallization.

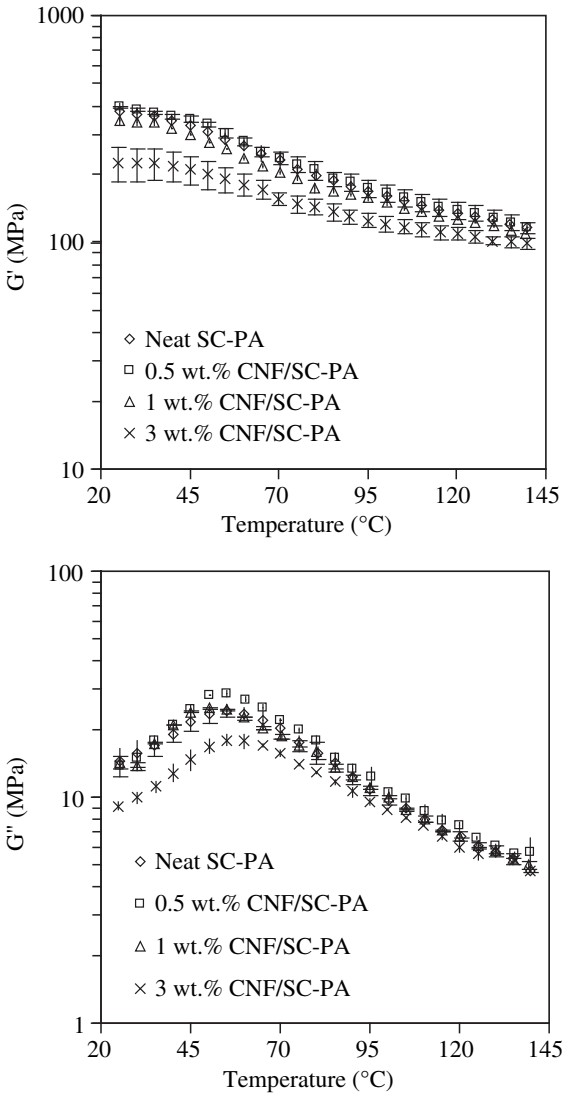

Fig. 5. DMA results of SC-PA materials. No distinct reinforcement of G′ was observed at any loading of CNFs. Similar to the A-PA matrix, reinforcement of G″ was observed in the vicinity of T_g for CNF loadings of 0.5 wt.% and 1 wt.%.

attributed to the addition of CNFs only. During crystallization, only the 0.5 wt.% CNF/A-PA composite possessed a greater value of G' that was distinct from the neat A-PA, and this material showed a maximum modulus improvement of 86% at 135 °C. The largest reinforcement to G'' occurred in the vicinity of the glass transition at 65 °C. The 0.5 wt.%, 1 wt.%, and 3 wt.% CNF composites showed increases of 94%, 88%, and 29%, respectively when compared to the neat A-PA. Similar to the values of G' during the crystallization event, only the 0.5 wt.% CNF/A-PA composite possessed a greater value of G'' than the neat A-PA during matrix crystallization.

Unlike the A-PA composites, none of the SC-PA composites showed any improvement in G' with the addition of CNFs as shown in Fig. 5. At a loading of 0.5 wt.%, the value of G' was the same as the neat SC-PA when considering experimental error, and the other two composites showed values that were consistently below the corresponding value of G' for the neat SC-PA. To understand these results more fully, first heating cycle data from DSC was analyzed for samples from the compression molded sheets used for DMA. Calculating the crystallinity of the polymer during the first heating cycle indicated the morphology of the tested samples. For the 3 wt.% CNF/SC-PA composite, first heating cycle data indicated that the crystallinity of the polymer in the composite was reduced with respect to the neat polymer sample. Whereas the neat polymer had 47% crystallinity, the 3 wt.% composite had 40% crystallinity. This difference clearly contributed to the decreased modulus measured in the DMA experiments for the 3 wt.% composite. The 0.5 wt.% and 1 wt.% CNF/SC-PA composites both had 48% crystallinity, so morphological changes would have had little to no effect on the moduli measured by DMA. Similar to the A-PA composites, the only distinct improvement seen in G'' was at temperatures slightly below T_g. The 0.5 wt.% CNF composite showed a 22% improvement in G'' at 50 °C, and the 1 wt.% CNF composite showed an 11% improvement at 45 °C.

4. Discussion

The results of the SEM imaging and DSC experiments provide a basis for understanding the DMA results. The SEM imaging showed that the CNFs were largely dispersed to the individual nanofiber level and homogeneously distributed in the fracture surfaces observed. Only one sample, 0.5 wt.%/SC-PA, showed any evidence of fiber aggregation, and this sample showed only one CNF agglomerate. From these results, we can assume that the CNF dispersion and distribution were common factors in each matrix system at a given CNF loading. The data obtained from the DSC experiments concerning T_g and melting behavior in both matrix systems show negligible impact of CNF addition on matrix morphology at all CNF loadings for the A-PA composites and at CNF loadings of 0.5 wt.% and 1 wt.% for the SC-PA composites. In this study, these results were ideal allowing us to treat the underlying matrix morphology as a constant at the CNF loadings specified above. These results simplify the data analysis and allow for the effect of matrix morphology on nanocomposite properties to be studied directly.

The DMA results indicated that at a CNF loading of less than 1 wt.%, the nanofibers were capable of providing reinforcement below T_g in the amorphous matrix and did not degrade the properties of the semi-crystalline matrix. At temperatures above T_g, no significant reinforcement was observed in either matrix system, indicating that negligible interfacial material was present. In fact, the increased value of G'' for the composites, with respect to the neat polymers close to T_g, indicated that the volume of constrained polymer in the composites was lower than the neat polymers' [4,36]. Loadings of 1 wt.% and higher did not provide any additional improvement, and in the case of the semi-crystalline matrix, the properties decreased with respect to the neat polymer with CNF addition at the highest two loadings studied here. Considering the 0.5 wt.% CNF composites, these results indicated that the reinforcement efficacy was higher in the amorphous matrix where individual chains can more efficiently accommodate the inclusion of nanofillers due to the lack of long range order and less restrictions on individual chain conformation.

To compare the DMA results between the two systems, micromechanical modeling was performed using the Halpin-Tsai equations for an isotropic composite containing discontinuous fibers [37]. The equations used are given below as Equations (1)–(5).

$$G_{\text{random}} = \frac{1}{8}E_{\text{L}} + \frac{1}{4}E_{\text{T}} \tag{1}$$

$$E_{\text{L}} = \frac{1 + 2(l/d)\eta_{\text{L}}V_{\text{f}}}{1 - \eta_{\text{L}}V_{\text{f}}}E_{\text{m}} \tag{2}$$

$$E_{\text{T}} = \frac{1 + 2\eta_{\text{T}}V_{\text{f}}}{1 - \eta_{\text{T}}V_{\text{f}}}E_{\text{m}} \tag{3}$$

$$\eta_L = \frac{\left(E_f/E_m\right) - 1}{\left(E_f/E_m\right) + 2(l/d)} \quad (4)$$

$$\eta_T = \frac{\left(E_f/E_m\right) - 1}{\left(E_f/E_m\right) + 2} \quad (5)$$

In these expressions, G_{random} is the shear modulus of the isotropic composite, E_L is the longitudinal elastic modulus of the composite, E_T is the transverse elastic modulus of the composite, E_f is the elastic modulus of the fiber, E_m is the elastic modulus of the matrix, l/d is the fiber aspect ratio, and V_f is the fiber volume fraction. The value of E_f was assumed to be 180 GPa [14]. In order to convert the matrix shear storage modulus to E_m, a value of 0.40 and 0.33 for Poisson's ratio of the A-PA and SC-PA were used, respectively [35]. The value of the fiber aspect ratio was taken as 100, and the volume fraction was calculated using a fiber density of 1.95 g/cm^3, A-PA density of 1.14 g/cm^3, and SC-PA density of 1.07 g/cm^3. All density values were obtained from the manufacturers. In these experiments, the value of G_{random} is compared to G' for the composites at 35 °C and 25 °C for the A-PA and SC-PA systems, respectively. The chosen temperature is approximately 30 °C below T_g in each system.

The model predictions for this system indicated that the A-PA matrix should experience a higher reinforcing efficacy from the addition of CNFs. The A-PA composites were predicted to show 18, 31 and 84% improvement with respect to the neat polymer at CNF loadings of 0.5 wt.%, 1 wt.%, and 3 wt.%, respectively. The SC-PA composites were predicted to show a lesser percentage of reinforcement with 9, 18, and 56% improvement at CNF loadings of 0.5 wt.%, 1 wt.%, and 3 wt.%, respectively. These results suggested that the matrix with the lower modulus (A-PA) should be affected to a greater extent by the rigid filler inclusion; thus, the modeling is qualitatively consistent with the experimental results between matrix systems. However, quantitative agreement was not obtained as shown in Table 2.

For the A-PA matrix composites, the agreement between the model and the experiment changed with CNF loading. At 0.5 wt.% CNF, the experimental value exceeded the modeling prediction by 15%. For the 1 wt.% CNF composite the experimental value and modeling prediction were approximately equal, and at the highest loading, the modeling prediction exceeded the experimental modulus value by 29%. For the SC-PA matrix composites, the experimental values were all below the modeling predictions. The model assumes that the matrix properties did not change with CNF addition, which was true for all of the materials tested here except the 3 wt.% CNF/SC-PA composite. Additionally, the model used a fixed fiber aspect ratio which may be adjusted arbitrarily, and we have assumed that the fiber aspect ratio was the same in both systems. The value that we have used in the model, 100, is the upper limit of aspect ratios observed in another melt-mixing study with CNF composites [30]. However the amount of reinforcement predicted by the model increased with increasing fiber aspect ratio, so this choice of aspect ratio led to the most conservative prediction. Considering the results and the assumptions of the model, the model predictions support the experimental findings in that a higher reinforcing efficacy was seen for the amorphous matrix.

Taken together, these results provide unique evidence that the bulk matrix morphology played an important role in the ultimate properties attained when a substantial interfacial zone was not present. These results are distinct from dramatic nanocomposites reinforcement reported at temperatures above T_g. In those studies [11,38–40], interfacial polymer chains were physically or chemically constrained at temperatures above where bulk polymer slippage was occurring, leading to substantial mechanical reinforcement beyond the levels observed here. The results of the experiments presented here are relevant to reinforcement behavior when the polymer chains are effectively immobile, and differences in the amorphous and semi-crystalline matrices may be attributed to the matrix directly. From these results, the conclusion may be drawn that amorphous matrices have the potential for higher relative mechanical reinforcement with low levels of nanofillers.

Table 2
Comparison of experimental and modeling results for DMA approximately 30 °C below T_g.

G′	CNF/A-PA composites			CNF/SC-PA composites		
	0.5 wt.%	1 wt.%	3 wt.%	0.5 wt.%	1 wt.%	3 wt.%
Experimental value (MPa)	288 ± 9	277 ± 29	279 ± 25	394 ± 2	342 ± 13	224 ± 39
Modeling prediction (MPa)	252	280	394	410	445	587

5. Conclusion

CNF nanocomposites with chemically similar but morphologically different polymer matrices were processed and characterized to understand the effect of bulk polymer morphology on properties. DSC analysis revealed that, under highly controlled cooling conditions, the addition of CNFs did not affect the matrix structure in both the amorphous and semi-crystalline matrices. The structure of the matrix from DMA results provided evidence that was qualitatively consistent with predictions from micromechanical modeling, leading to the conclusion that amorphous matrices have the potential for higher reinforcement with respect to semi-crystalline matrices at the same nanofiller loading. This higher reinforcement was largely independent from any contributions of interfacial material since the composites had a similar modulus to the neat polymer in both systems above T_g. A lack of high temperature reinforcement suggested that the interaction between the components was not strong and a lower volume of constrained polymer was indicated by the increased value of G'' in the composites. Overall, these results provided new insight into the nature of nanocomposite reinforcement below T_g and another means for designing nanocomposite mechanical properties.

Acknowledgements

The authors gratefully acknowledge financial support from the Ralph E. Powe Junior Faculty Enhancement Award provided by Oak Ridge Associated Universities and from Solvay Advanced Polymers. X. Hu was supported by a fellowship from the State Scholarship Fund of China during her appointment at Georgia Tech. The authors also appreciate donations of materials from Pyrograf Products, Shakespeare Polymers, and Sun Plastech.

References

[1] Fukushima Y, Inagaki S. Journal of Inclusion Phenomena 1987;5(4):473–82.
[2] Fukushima Y, Okada A, Kawasumi M, Kurauchi T, Kamigaito O. Clay Minerals 1988;23(1):27–34.
[3] Usuki A, Kojima Y, Kawasumi M, Okada A, Fukushima Y, Kurauchi T, et al. Journal of Materials Research 1993;8(5):1179–84.
[4] Kojima Y, Usuki A, Kawasumi M, Okada A, Fukushima Y, Kurauchi T, et al. Journal of Materials Research 1993;8(5):1185–9.
[5] Iijima S. Nature 1991;354(6348):56–8.

[6] Ash BJ, Siegel RW, Schadler LS. Journal of Polymer Science, Part B: Polymer Physics 2004;42(23):4371–83.
[7] Bansal A, Yang H, Li C, Cho K, Benicewicz BC, Kumar SK, et al. Nature Materials 2005;4(9):693–8.
[8] Mitchell CA, Bahr JL, Arepalli S, Tour JM, Krishnamoorti R. Macromolecules 2002;35(23):8825–30.
[9] Mackay ME, Dao TT, Tuteja A, Ho DL, Van Horn B, Kim H-C, et al. Nature Materials 2003;2(11):762–6.
[10] Geng H, Rosen R, Zheng B, Shimoda H, Fleming L, Liu J, et al. Advanced Materials 2002;14(19):1387–90.
[11] Sternstein SS, Zhu A-J. Macromolecules 2002;35(19):7262–73.
[12] Shofner ML, Khabashesku VN, Barrera EV. Chemistry of Materials 2006;18(4): 906–13.
[13] Li J, Fang ZP, Tong LF, Gu AJ, Liu F. Journal of Applied Polymer Science 2007;106(5):2898–906.
[14] Uchida T, Anderson DP, Minus ML, Kumar S. Journal of Materials Science 2006;41(18):5851–6.
[15] Shofner ML, Lozano K, Rodriguez-Macias FJ, Barrera EV. Journal of Applied Polymer Science 2003;89(11):3081–90.
[16] Shofner ML, Rodriguez-Macias FJ, Vaidyanathan R, Barrera EV. Composites Part A: Applied Science and Manufacturing 2003;34(12):1207–17.
[17] Tibbetts GG, McHugh JJ. Journal of Materials Research 1999;14(7):2871–80.
[18] Finegan IC, Tibbetts GG. Journal of Materials Research 2001;16(6):1668–74.
[19] Glasgow DG, Lake ML, Tibbetts GG, Finegan JC, Kwag C. Carbon nanofiber surface treatment effects on polypropylene composite properties. In: Tolle TB, Larson BK, editors. SAMPE-ACCE-DOE advanced materials conference proceedings. Detroit, Michigan: Society for the Advancement of Material and Process Engineering; 1999. p. 156–63.
[20] Lozano K, Barrera EV. Journal of Applied Polymer Science 2001;79(1):125–33.
[21] Lozano K, Bonilla-Rios J, Barrera EV. Journal of Applied Polymer Science 2001;80(8):1162–72.
[22] Ma HM, Zeng JJ, Realff ML, Kumar S, Schiraldi DA. Composites Science and Technology 2003;63(11):1617–28.
[23] Kumar S, Rath T, Mahaling RN, Reddy CS, Das CK, Pandey KN, et al. Materials Science and Engineering B 2007;141(1–2):61–70.
[24] Isayev AI, Jung C, Gunes K, Kumar R. International Polymer Processing 2008;23(4):395–405.
[25] Lozano K, Yang S, Jones RE. Carbon 2004;42(11):2329–31.
[26] Yang S, Taha-Tijerina J, Serrato-Diaz V, Hernandez K, Lozano K. Composites Part B-Engineering 2007;38(2):228–35.
[27] Zeng JJ, Saltysiak B, Johnson WS, Schiraldi DA, Kumar S. Composites Part B-Engineering 2004;35(3):245–9.
[28] Park SJ, Im SH, Lee JR, Rhee JM. Polymer-Korea 2006;30(5):385–90.
[29] Jimenez GA, Jana SC. Composites Part A: Applied Science and Manufacturing 2007;38(3):983–93.
[30] Wang Y, Xu J, Bechtel SE, Koelling KW. Rheologica Acta 2006;45(6):919–41.
[31] Morales-Teyssier O, Sanchez-Valdes S, Ramos-de Valle LF. Macromolecular Materials and Engineering 2006;291(12):1547–55.
[32] Cipriano BH, Kota AK, Gershon AL, Laskowski CJ, Kashiwagi T, Bruck HA, et al. Polymer 2008;49(22):4846–51.
[33] Kelarakis A, Yoon K, Somani R, Sics I, Chen XM, Hsiao BS, et al. Polymer 2006;47(19):6797–807.
[34] Lozano K, Files B, Rodríguez-Macías FJ, Barrera EV. Purification and functionalization of vapor grown carbon nanotubes and single wall nanotubes. In: Powder materials: current research and industrial practice (TMS fall meeting proceedings). Cincinnati, Ohio; 1999. pp. 333–40.
[35] Mehta RH. Physical constants of various polyamides. In: Brandrup J, Immergut EH, Grulke EA, Abe A, Bloch DR, editors. Polymer handbook. New York: John Wiley and Sons, Inc.; 2005.
[36] Oka S, Chikahisa Y. Kobunshi bussei. Tokyo: Asakura Syoten; 1974.
[37] Agarwal BD, Broutman LJ. Analysis and performance of fiber composites. 2nd ed. New York: John Wiley and Sons; 1990.
[38] Zhu ZY, Thompson T, Wang S-Q, von Meerwall ED, Halasa A. Macromolecules 2005;38(21):8816–24.
[39] Havet G, Isayev AI. Rheologica Acta 2003;42(1–2):47–55.
[40] Kaur J, Shofner ML. Macromolecular Chemistry and Physics 2009;210(8):677–88.